MATERIAL SPECIFIC MULTIPLE OBSERVATION RESOLUTION ENHANCEMENT OF HYPERSPECTRAL IMAGERY

Toygar Akgun and Yucel Altunbasak

Center for Signal and Image Processing
Georgia Institute of Technology
Atlanta, Georgia, 30332-0250

ABSTRACT

In [1] we proposed a hyperspectral imaging model that represents spectral observations at different wavelengths as weighted linear combinations of a small number of basis images obtained through principal component analysis (PCA). Based on this imaging model we formulated a multiple observation resolution enhancement method for hyperspectral imagery. In this work we focus on *material specific* resolution enhancement. We start with pointing out a shortcoming of the PCA based imaging model. We then introduce modifications to integrate linear spectral mixing into the imaging model. Based on the updated model we introduce and implement material specific multiple observation resolution enhancement for hyperspectral imagery. We test the proposed method on AVIRIS data, and present numeric and visual results.

Index Terms— Hyperspectral imagery, linear mixing, endmember, spatial resolution enhancement.

1. INTRODUCTION

In [1] we proposed a hyperspectral imaging model that represents spectral observations at different wavelengths as weighted linear combinations of a small number of basis images obtained through principal component analysis (PCA). Based on this imaging model we formulated a multiple observation resolution enhancement method for hyperspectral imagery. In many hyperspectral imagery applications, dimensionality reduction through PCA is an integral component of the solution. The reason is two-fold: First, limitations on the computational budget may dictate dimensionality reduction. Second, in many applications final results are reported to a human observer who can not handle the full dimensionality of hyperspectral data, and dimensionality reduction is required to render efficient interpretation possible. Hence, integration of PCA into the resolution enhancement framework makes sense. The hyperspectral superresolution technique proposed in [1] simultaneously reduces dimensionality, suppresses undesired noise and performs resolution enhancement on the transformed data.

However, in certain applications, such as mining and petroleum exploration, we are interested in detecting specific materials with well-defined spectral signatures. Although PCA is an effective dimensionality reduction tool, it can not emphasize individual spectral signatures of interest. This is a direct result of the fact that principal components represent the highest variance (information) as a linear combination of multiple spectral signatures. For example, in military applications, such as enemy ground observation, camouflaged vehicles may not be directly recognizable if observed in the main principle component. But if we consider the bands that represent certain metal or alloys known to constitute such vehicles, detection problem is greatly alleviated. Hence, if we are interested only in a specific spectral signature, then all the other materials in the scene can be considered as interference, and integrating PCA within the observation model does not make sense. These observations lead to the idea of material specific hyperspectral superresolution.

2. LINEAR MIXING BASED IMAGING MODEL

Typical hyperspectral pixels are not *pure* in terms of spectral content, meaning that each hyperspectral pixel is a combination of several different spectral signatures. Such pixels are called *mixed* pixels, as opposed to the pure pixels that consist of a single unique spectral signature. Mixed pixels exist for one of two reasons. First, the typical spatial resolution of hyperspectral sensors are in the scale of tens of meters. Hence, the spatial coverage of each pixel may include several different materials with different spectral signatures. Second, regardless of the spatial resolution, distinct materials can be found as homogenous mixtures. Due to this spectral mixing phenomenon, hyperspectral pixels are frequently analyzed in terms of *spectral mixing models*. Mixing models represent the acquired hyperspectral pixels as combinations of a limited number of constituent spectral endmembers, where spectral endmembers are defined as spectrally pure features such as vegetation, soil, etc. Spectral signatures of pure endmembers are usually defined under idealized laboratory conditions with controlled illumination. Although this is a perfectly valid ap-

1-4244-1484-9/08/$25.00 ©2008 IEEE

proach to obtain spectral endmembers, spectral signatures obtained in controlled laboratory conditions can not reflect the atmospheric effects present in field data. To overcome this shortcoming endmember signatures can be extracted directly from the observed data. This task is referred to as *endmember extraction*, and is typically based on certain properties of the endmembers. For a detailed treatment of endmember extraction please refer to [2].

Spectral mixing models provide the foundation for analyzing and processing hyperspectral data. Current mixing models are based on the simple assumption that within a given scene, the surface is dominated by a small number of endmembers. The fractions endmembers appear in a mixed pixel are called *fractional abundances*. Based on this assumption, observed pixels are modeled as combinations of these endmembers. Depending on how the combination mechanism is modeled, different mixing models result. The most popular mixing model, namely, the linear mixing model (LMM), assumes that the observed pixels can be represented as linear combinations of deterministic endmembers. Given a mixing model and the endmembers present in an observed scene, the task of estimating fractional abundances is referred to as *spectral unmixing*. For a detailed treatment of spectral mixing please refer to [2].

The first step in applying the hyperspectral image acquisition model to material specific superresolution is to integrate a linear spectral mixing model into the current framework. For our purposes any linear mixing model is applicable. Once we have an observation model that relates the observed hyperspectral pixels to the endmembers and spatially aliased abundance maps, we can move to superresolution. We shall start with presenting a projection operator that optimally filters out undesired spectral signatures, and apply superresolution on the resulting projected data. The main idea is to project each hyperspectral pixel onto a subspace orthogonal to the undesired signatures. This operation can be shown to be an optimal interference suppression process in the least squares sense [3]. Once the interfering signatures have been nulled, we project the residual onto the signatures of interest and perform superresolution of the resulting image planes. This operation maximizes the SNR, and results in a small number of resolution enhanced images of materials that we are interested in.

Let us denote the spatially and spectrally continuous hyperspectral pixel with $f(x_1, x_2, \lambda, k)$. Then within the limitations of linear mixing model, we have

$$f(x_1, x_2, \lambda, k) = \sum_{j=1}^{M} e_j(\lambda) f_j(x_1, x_2, k), \tag{1}$$

where x_1 and x_2 are the continuous spatial variables, k is the observation index, λ is the continuous wavelength, and $e_j(\lambda)$ denotes the j^{th} endmember. Comparing Eq. (1) with the results of [1] we see that the derivations presented in [1] are exactly applicable if we but replace the spectral PCA basis functions $b_j(\lambda)$ with the spectral endmembers $e_j(\lambda)$. Hence, the observed pixels can be represented as

$$\begin{aligned} g_i[m_1, m_2, k] = \sum_{j=1}^{P} s_{i,j} \sum_{n_1=0}^{N_1-1} \sum_{n_2=0}^{N_2-1} f_j[n_1, n_2, k_r] \\ \times h_b[m_1, m_2; n_1, n_2; k; k_r] + v[m_1, m_2, k], \end{aligned}$$

where $s_{i,j}$ is defined as

$$s_{i,j} \doteq \int_0^\infty e_j(\lambda) r_i(\lambda)\, d\lambda.$$

In matrix-vector form

$$\boldsymbol{g}[\boldsymbol{m}, k] = \boldsymbol{S}\boldsymbol{H}\boldsymbol{f}[\boldsymbol{m}, k] + \boldsymbol{v}[\boldsymbol{m}, k], \tag{2}$$

where the following shorthand notations are used simplify the expression:

$$\boldsymbol{g}[\boldsymbol{m}, k] \doteq \begin{bmatrix} g_1[\boldsymbol{m}, k] \\ g_2[\boldsymbol{m}, k] \\ \vdots \\ g_Q[\boldsymbol{m}, k] \end{bmatrix}, \quad \boldsymbol{f}[\boldsymbol{n}, k_r] \doteq \begin{bmatrix} \boldsymbol{f}_1[\boldsymbol{n}, k_r] \\ \boldsymbol{f}_2[\boldsymbol{n}, k_r] \\ \vdots \\ \boldsymbol{f}_P[\boldsymbol{n}, k_r] \end{bmatrix},$$

$$\boldsymbol{H}\boldsymbol{f}[\boldsymbol{m}, k] \doteq \begin{bmatrix} \boldsymbol{f}_1[\boldsymbol{n}, k_r] \cdot \boldsymbol{h}_b[\boldsymbol{m}; \boldsymbol{n}; k; k_r] \\ \boldsymbol{f}_2[\boldsymbol{n}, k_r] \cdot \boldsymbol{h}_b[\boldsymbol{m}; \boldsymbol{n}; k; k_r] \\ \vdots \\ \boldsymbol{f}_P[\boldsymbol{n}, k_r] \cdot \boldsymbol{h}_b[\boldsymbol{m}; \boldsymbol{n}; k; k_r] \end{bmatrix},$$

$$\boldsymbol{S} \doteq \begin{bmatrix} s_{1,1} & \cdots & s_{1,6} \\ s_{2,1} & \cdots & s_{2,6} \\ \vdots & \ddots & \vdots \\ s_{Q,1} & \ldots & s_{Q,6} \end{bmatrix}, \quad \boldsymbol{v}[\boldsymbol{m}, k] \doteq \begin{bmatrix} v_1[\boldsymbol{m}, k] \\ v_2[\boldsymbol{m}, k] \\ \vdots \\ v_Q[\boldsymbol{m}, k], \end{bmatrix}$$

$$\begin{aligned} \boldsymbol{f}_j[\boldsymbol{n}, k_r] \cdot \boldsymbol{h}_b[\boldsymbol{m}; \boldsymbol{n}; k; k_r] \doteq \sum_{n_1=0}^{N_1-1} \sum_{n_2=0}^{N_2-1} f_j[n_1, n_2, k_r] \\ \times h_b[m_1, m_2; n_1, n_2; k; k_r]. \end{aligned}$$

Here Q denotes the number of observed spectral bands, and P denotes the number of endmembers in the observed scene.

The similarity between inverting Eq. (2) and the spectral unmixing problem is worth noting. If we choose the downsampling ratio as one, that is, if we assume the target and observed images are at the same spatial resolution, then the resulting problem is equivalent to spectral unmixing with multiple registered observations. The main advantage of such an approach would be the increased robustness against observation noise provided by multiple observations for each pixel location (as a result of spatial registration). When the target image is of higher resolution, the resulting problem is similar to the problem described in [1]. By using a POCS based iterative inversion algorithm similar to the algorithm outlined in [1] we could obtain a superresolved abundance map that would be valuable for subpixel target detection. However, we will concentrate on superresolving the abundance map of a single endmember by incorporating an additional step into the imaging model.

3. MATERIAL SPECIFIC PROJECTION

Without losing any generality, let us assume that we are interested on a single endmember. All the derivations to follows can be easily extended to multiple endmembers. Superresolving a specific endmember is complicated by the correlation between endmembers and the presence of noise. A direct correlation-based approach by projecting the observed pixels on the endmember of interest is suboptimal [3]. To see this, note that along with noise, all the endmembers we are not interested act as interference, and the correlation between the target endmember and these undesired endmembers can be quite high, at least in certain spectral bands. We can achieve better results if we project the observed hyperspectral pixels onto a custom designed subspace. Let us start with the effects of the interfering spectral signatures. Note that the columns of the $\boldsymbol{S}$ matrix are the endmembers after the application of spectral filtering. We can rearrange columns of $\boldsymbol{S}$ so that the endmember of interest is the first column: $\boldsymbol{S} = [\boldsymbol{d} \quad \boldsymbol{U}]$. Here the column vector $\boldsymbol{d}$ is the desired endmember and $\boldsymbol{U}$ is the matrix consisting of interfering endmembers. To eliminate the effects of the interfering endmembers, we will apply the technique proposed in [3]. The main idea is to project the observed hyperspectral signature onto the a subspace that is orthogonal to all interfering spectral signatures. This is equivalent to projecting onto the nullspace of $\boldsymbol{U}^T$. We use a classic result from linear algebra to write the least squares optimal projection operator as

$$\boldsymbol{P} = \boldsymbol{I} - \boldsymbol{U}\boldsymbol{U}^{\dagger},$$

where $\boldsymbol{U}^{\dagger}$ denotes the pseudoinverse of $\boldsymbol{U}$. If $\boldsymbol{U}$ is full-column rank then $\boldsymbol{U}^{\dagger} = (\boldsymbol{U}^T\boldsymbol{U})^{-1}\boldsymbol{U}^T$. The resulting vector will only have energy coming from the desired spectral signature and noise. The application of $\boldsymbol{P}$ effectively removes contribution from the columns of $\boldsymbol{U}$, that is,

$$\boldsymbol{P}\boldsymbol{g} = \boldsymbol{P}\boldsymbol{d}\tilde{f}_d + \boldsymbol{P}\boldsymbol{v},$$

where $\tilde{f}_d$ is the element of the vector $\boldsymbol{H}\boldsymbol{f}$ that corresponds to the desired endmember. The next step is to minimize the effect of remaining noise component. Let us denote the operator that maximizes SNR with $\boldsymbol{q}^T$. Then we have

$$\boldsymbol{q}^T\boldsymbol{P}\boldsymbol{g} = \boldsymbol{q}^T\boldsymbol{P}\boldsymbol{d}\tilde{f}_d + \boldsymbol{q}^T\boldsymbol{P}\boldsymbol{v}. \tag{3}$$

Using the results of the well-studied generalized eigenvalue problem [4], we can show that

$$\boldsymbol{q}^T = \kappa\boldsymbol{d}^T,$$

where κ is an arbitrary constant. Finally, the combination of these two projection operators gives the least squares optimal projection operator we desire, that is,

$$\boldsymbol{Q} = \boldsymbol{q}^T\boldsymbol{P} = \kappa\boldsymbol{d}^T\boldsymbol{P}. \tag{4}$$

For a detailed treatment of the derivation (for single and multiple spectral signatures of interest) and computation of the projection operator please refer to [3], [4] and the references therein.

From Eq. (4) and Eq. (3) we can see that upon application of the proposed projection operator we are left with the conventional superresolution setup. We have a number of warped, aliased and noisy single-plane abundance maps of a predetermined endmember, and our goal is to obtain a superresolved single-plane abundance map. This inverse problem can be solved with any of the superresolution algorithms proposed in literature. We preferred to use the POCS based technique detailed in [5].

4. RESULTS

To test the proposed method we require ground truth hyperspectral data with a complete set of endmembers and corresponding fractional abundances. Such ground truth data is very hard, if possible at all, to obtain. We could pick spectral signatures from existing endmember libraries, and synthesize pixels by linearly combining these signatures with random weights. This is a feasible approach for obtaining numeric results, but it becomes very cumbersome if we want to provide visual results with meaningful spatial structure. To get around this obstacle we used the following approach. We started with the AVIRIS reflectance data set used in [1]. We first applied the technique proposed in [6] to extract the endmembers shown in Figure 1. Then assuming the linear mixing model, we applied the nonnegative least squares (NNLS) method summarized in [2] to estimate the fractional abundance maps for all endmembers. Since the extracted endmembers can never perfectly match the true endmembers in the scene [2] the obtained fractional abundance maps can not represent the data with zero (or negligibly small) error. To have a scene with perfectly matching endmembers and abundance maps, we synthesized a new hyperspectral data set using the computed fractional abundance maps and the extracted spectral endmembers under the linear mixing model. All experiments presented in this section are conducted on this synthesized data. Note that the validity of our results is not dependent on the specific endmember extraction technique used. For all practical purposes, we could have even assumed that the endmembers were given. But for the data set we picked, such predetermined endmembers and corresponding abundance maps were not available at the time we conducted our experiments.

For the visual results demonstrated in Figure (2) the fourth endmember shown in Figure 1 is used. The optimal subspace

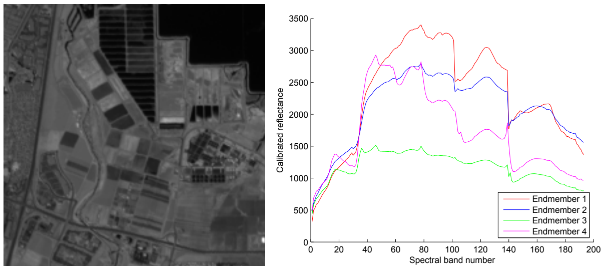

Fig. 1. 100^{th} band of the original scene and extracted endmembers

	AVIRIS Reflectance Data	
	Bilinear interpolation	Proposed method
Case 1 (Noise free)	21.07	26.71
Case 2 (AWGN $\sigma = 30$)	19.77	21.34

Table 1. Numerical results for AVIRIS reflectance data with and without noise.

projection based superresolution method is compared to bilinearly interpolating the abundance map obtained by applying the proposed projection operator on a single low resolution observation. We assume global translational motion scenario simulated by capturing spatially shifted windows. The shifted windows are spatially blurred with a Gaussian blur filter with unit variance and downsampled by three in both spatial dimensions. For spatial noise we experimented with two cases, namely, noise free (Case 1) and additive white Gaussian noise (AWGN) with a standard deviation of 30 (Case 2). For the sake of simplicity we ignored spectral blurring effects.

Numerical results in terms of $PSNR$ are given in Table (1). We can see that the proposed method clearly outperforms bilinear interpolation. Visual results presented in Figure (2) also confirm the improvement seen in $PSNR$ values. The proposed method effectively suppresses the effects of interfering spectral signatures and noise, and achieves spatial resolution enhancement.

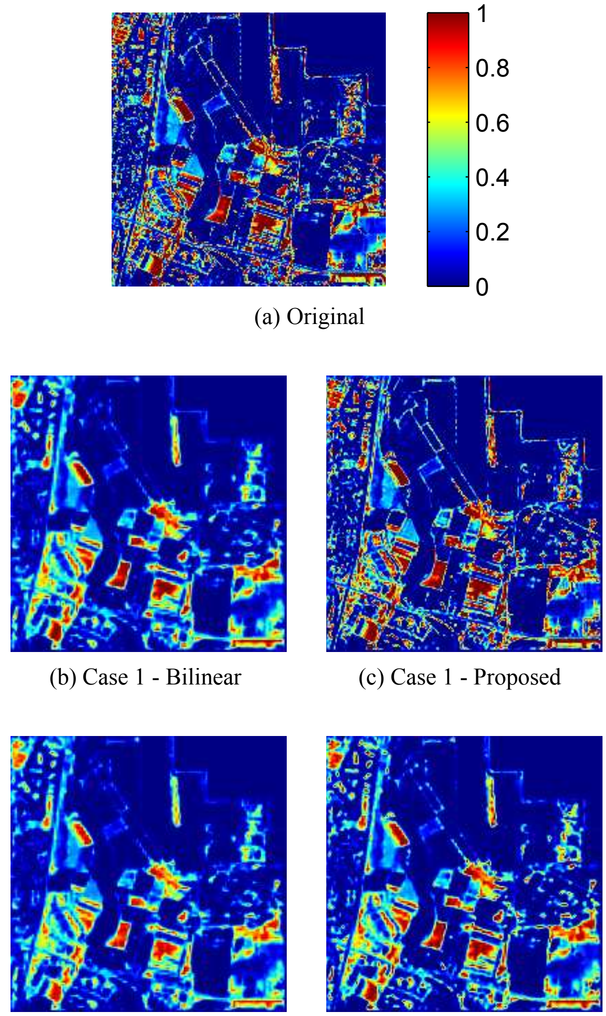

(a) Original

(b) Case 1 - Bilinear

(c) Case 1 - Proposed

(d) Case 2 - Bilinear

(e) Case 2 - Proposed

Fig. 2. Results for the first **reflectance** test image extracted from 224-band Moffett Field (AVIRIS Reflectance Data - 1).

5. REFERENCES

[1] T. Akgun, Y. Altunbasak, and R. M. Mersereau, “Super-resolution reconstruction of hyperspectral images,” *IEEE Transactions on Image Processing*, vol. 14, no. 11, pp. 1860–1875, Nov 2005.

[2] N. Keshava and J.F. Mustard, “Spectral unmixing,” *IEEE Signal Processing Magazine*, vol. 19, pp. 44–57, Jan. 2002.

[3] J. C. Harsanyi and C. Chang, “Hyperspectral image classification and dimensionality reduction: An orthogonal subspace projection approach,” *IEEE Transactions on Geoscience and Remote Sensing*, vol. 32, no. 4, pp. 779–785, July 1994.

[4] J. W. V. Miller, J. B. Farison, and Y. Shin, “Spatially invariant image sequences,” *IEEE Transactions on Image Processing*, vol. 1, pp. 148–161, Apr. 1992.

[5] Y. Altunbasak, A.J. Patti, and R.M. Mersereau, “Super-resolution still and video reconstruction from MPEG-coded video,” *IEEE Transactions on Circuits and Systems for Video Technology*, vol. 12, no. 4, pp. 217–226, 2002.

[6] A. D. Stocker and Alan Schaum, “Application of stochastic mixing models to hyperspectral detection problems,” in *Proc. SPIE Algorithms for Multispectral and Hyperspectral Imagery III*, Istanbul, Turkey, June 2000.